Lagrangian Formulation of a Spring Pendulum with Oscillating Magnetic Interaction

Contents

1   System Description

We consider a spring pendulum system where:

- A mass m is attached to a spring with a spring constant k and natural length l_0.

- The mass is free to move in both radial (r) and angular (θ) directions.

- The mass is ferromagnetic with a magnetic moment μ, and is influenced by an oscillating magnetic field $B(t)$.

- The system is also subject to gravity, with gravitational acceleration g.
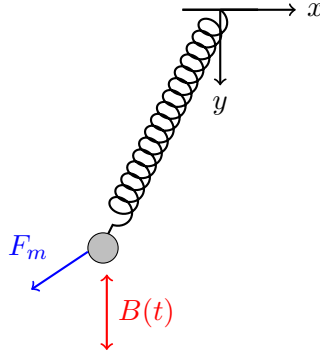
Figure 1: A diagram of the spring pendulum system with a ferromagnetic mass influenced by an oscillating magnetic field. The mass is attached to the end of the spring, which extends from the fixed support. The mass interacts with the oscillating magnetic field $B(t)$, depicted by a red arrow. The blue arrow represents the magnetic force F_m, which affects the angular motion. .

1.1   Generalized Coordinates

The system is described by the following coordinates:

- $r(t)$: The length of the spring.

- $\theta(t)$: The angular displacement of the pendulum from the vertical.

1.2   Kinetic Energy

The velocity of the mass can be expressed as:

$$v^2 = \dot{r}^2 + r^2\dot{\theta}^2$$

Thus, the kinetic energy is:

$$T = \frac{1}{2}m\left(\dot{r}^2 + r^2\dot{\theta}^2\right)$$

1.3 Potential Energy

The potential energy includes:

1. **Gravitational Potential:**
$$U_g = -mgr \cos \theta$$

2. **Spring Potential:**
$$U_s = \frac{1}{2}k(r - l_0)^2$$

3. **Magnetic Interaction:** Assuming the magnetic field oscillates as $B(t) = B_0 \cos(\omega t)$, the magnetic potential energy is:
$$U_m = -\mu B(t) \cos \theta = -\mu B_0 \cos(\omega t) \cos \theta$$

The total potential energy is:
$$U = -mgr \cos \theta + \frac{1}{2}k(r - l_0)^2 - \mu B_0 \cos(\omega t) \cos \theta$$

1.4 Lagrangian

The Lagrangian is defined as:
$$\mathcal{L} = T - U$$

Substituting the expressions for T and U:
$$\mathcal{L} = \frac{1}{2}m\left(\dot{r}^2 + r^2\dot{\theta}^2\right) + mgr \cos \theta - \frac{1}{2}k(r - l_0)^2 + \mu B_0 \cos(\omega t) \cos \theta$$

2 Equations of Motion

The equations of motion are derived using the Euler-Lagrange equations:
$$\frac{d}{dt}\left(\frac{\partial \mathcal{L}}{\partial \dot{q}_i}\right) - \frac{\partial \mathcal{L}}{\partial q_i} = 0$$

where q_i are the generalized coordinates.

2.1 Radial Motion (r)
$$m\ddot{r} - mr\dot{\theta}^2 + k(r - l_0) - mg \cos \theta = 0$$

2.2 Angular Motion (θ)
$$\frac{d}{dt}\left(mr^2\dot{\theta}\right) + mgr \sin \theta - \mu B_0 \cos(\omega t) \sin \theta = 0$$

3   Numerical Options and Methodology

the following section provides an overview of numerical methods for solving the coupled differential equations derived from the Lagrangian formulation. The equations of motion for the radial (r) and angular (θ) directions involve time-dependent terms, nonlinear coupling, and periodic forcing due to the oscillating magnetic field and therefore, robust numerical schemes are essential to ensure stability, accuracy, and computational efficiency. this section concludes with reasoning behind the final numerical choice made for this particular system.

4   Possible Numerical Schemes

4.1   Euler Method

The Euler method is a straightforward first-order numerical scheme. Given an ordinary differential equation (ODE) of the form:

$$\frac{dy}{dt} = f(t, y),$$

the Euler method approximates the solution as:

$$y_{n+1} = y_n + h f(t_n, y_n),$$

where h is the time step size. While simple to implement, the Euler method is conditionally stable and can accumulate significant numerical error, especially for stiff or oscillatory systems.

4.2   Verlet Integration

Verlet integration is widely used for conservative systems. It approximates the position and velocity using:

$$r_{n+1} = 2r_n - r_{n-1} + h^2 a_n,$$

where a_n is the acceleration at time step n. This method is second-order accurate, time-reversible, and conserves energy over long simulations. However, it is less efficient when velocity-dependent terms are present.

4.3   Runge-Kutta Methods (RK4 and RK45)

The fourth-order Runge-Kutta (RK4) method provides a high degree of accuracy. It updates the solution as:

$$y_{n+1} = y_n + \frac{h}{6}(k_1 + 2k_2 + 2k_3 + k_4),$$

where:

$$k_1 = f(t_n, y_n), \quad k_2 = f\left(t_n + \frac{h}{2}, y_n + \frac{h}{2}k_1\right),$$

$$k_3 = f\left(t_n + \frac{h}{2}, y_n + \frac{h}{2}k_2\right), \quad k_4 = f(t_n + h, y_n + hk_3).$$

The adaptive version (RK45) dynamically adjusts h based on error estimates, making it more efficient for varying dynamics.

4.4 Implicit Backward Euler Method

The backward Euler method is a first-order implicit scheme, given by:

$$y_{n+1} = y_n + hf(t_{n+1}, y_{n+1}).$$

This method is unconditionally stable and effective for stiff systems, but requires iterative solvers to handle the implicit nature.

4.5 Crank-Nicolson Method

The Crank-Nicolson method combines forward and backward Euler schemes:

$$y_{n+1} = y_n + \frac{h}{2} \left[f(t_n, y_n) + f(t_{n+1}, y_{n+1}) \right].$$

This second-order implicit method is stable and accurate for oscillatory systems.

4.6 Leapfrog Method

The leapfrog method updates positions and velocities alternately:

$$r_{n+1} = r_n + hv_{n+1/2}, \quad v_{n+3/2} = v_{n+1/2} + ha_{n+1}.$$

It is time-reversible, energy-conserving, and suitable for conservative systems, but less effective for systems with strong damping or stiffness.

4.7 Symplectic Integrators

Symplectic integrators, such as the velocity Verlet or implicit midpoint rule, are designed for Hamiltonian systems. For the implicit midpoint rule:

$$y_{n+1} = y_n + hf\left(\frac{t_n + t_{n+1}}{2}, \frac{y_n + y_{n+1}}{2} \right).$$

These methods preserve energy and momentum over long simulations but require implicit solvers.

4.8 Exponential Integrators

Exponential integrators solve linear components of ODEs analytically using:

$$y_{n+1} = e^{Ah} y_n + \int_0^h e^{A\tau} g(y_n) d\tau,$$

where A represents the linear operator. These methods are ideal for oscillatory systems or systems with stiffness.

4.9 Multiscale Methods

Multiscale methods address systems with multiple timescales by separating fast and slow dynamics. The heterogeneous multiscale method (HMM) is one example, where a reduced model is used for the slow dynamics, while the fast dynamics are simulated only as needed.

4.10   Geometric Integrators

Geometric integrators, such as discrete gradient methods, preserve invariants like energy or angular momentum. These methods are particularly useful for long-term simulations of conservative systems.

4.11   Methodology Selection

Considering the nonlinear coupling, oscillatory dynamics, and periodic forcing in the spring pendulum system:

- RK4 is the preferred choice for its high accuracy and efficiency in solving nonlinear systems.

- Adaptive RK45 is recommended for simulations with varying dynamics or fast transitions.

- Symplectic integrators are suitable for long-term energy conservation in undamped or weakly damped systems.

Based on these considerations:

1. The Euler method is unsuitable due to its low accuracy and conditional stability.

2. Verlet integration is effective for conservative dynamics but less ideal for velocity-dependent damping or magnetic forces.

3. The RK4 method offers high accuracy and is appropriate for the nonlinear coupled equations of motion, making it the preferred choice.

4. Implicit methods, such as backward Euler or Crank-Nicolson, are robust but computationally expensive due to the implicit nature.

5. The leapfrog method is suitable for conservative dynamics but less flexible for velocity-dependent forces.

Thus, the fourth-order Runge-Kutta method (RK4) is selected for its balance between accuracy, stability, and computational efficiency.

5   Simple Intial Conditions and Magnetic Field: Numerical Results and Visualizations

The numerical simulation of the spring pendulum system with magnetic interaction was performed using the fourth-order adaptive Runge-Kutta method (RK45). The system's dynamics were visualized using animations, phase portraits, and a Poincaré map, as described below.

This first set of results is created using a simplistic magnetic field, see Python code at `https://github.com/Leigh-Herman/Enhanced-Magnetic-Pendulum/blob/main/Magnetic_Pendulum.py`.

5.1 Animation of the System Dynamics

A GIF animation was created to visualize the motion of the spring pendulum over time. The animation captures:

- The oscillatory motion of the mass in the radial and angular directions.

- The periodic forcing due to the oscillating magnetic field.

- Real-time display of the system's configuration, including the spring and pendulum motion.

The animation provides an intuitive understanding of the coupled dynamics of the system, highlighting the influence of the magnetic field and nonlinear coupling. The GIF file is named `spring_pendulum.gif` which can be found in my GitHub `https://github.com/Leigh-Herman/Enhanced-Magnetic-Pendulum/blob/main/spring_pendulum.gif`.

5.2 Radial Phase Portrait

The radial phase portrait, shown in Figure **??**, plots the spring length (r) versus its radial velocity ($\dot{r}$):

$$\text{Radial Phase Portrait:} \quad r \text{ vs. } \dot{r}.$$

This visualization highlights the oscillatory behavior in the radial direction, showing the cyclic nature of the spring's extension and compression.
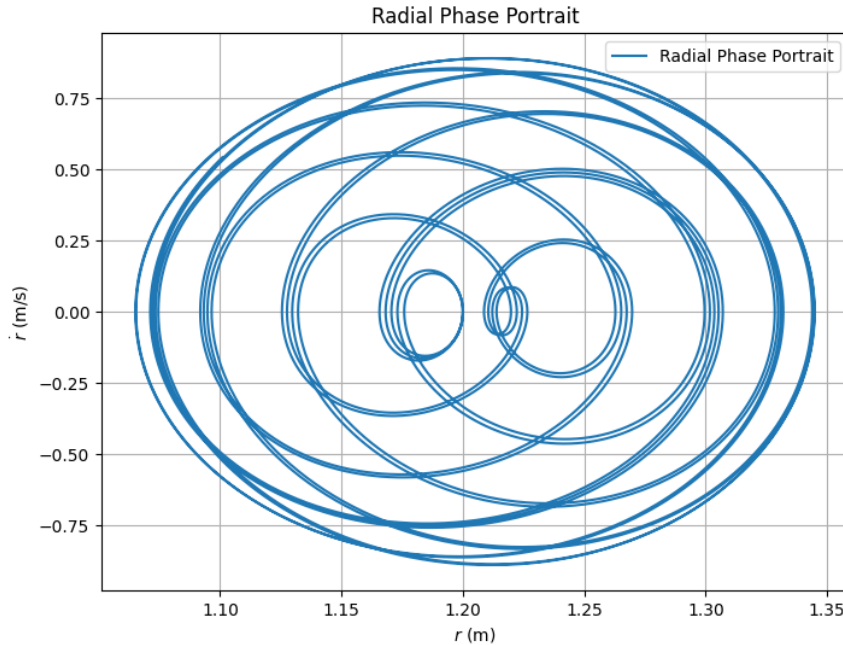

Figure 2: Radial phase portrait showing the relationship between the spring length r and its radial velocity $\dot{r}$.

5.3 Angular Phase Portrait

The angular phase portrait, shown in Figure **??**, plots the angular displacement (θ) versus its angular velocity ($\dot{\theta}$):

$$\text{Angular Phase Portrait:} \quad \theta \text{ vs. } \dot{\theta}.$$

This plot captures the periodic nature of the pendulum's angular motion, including the influence of the nonlinear coupling and magnetic forcing.
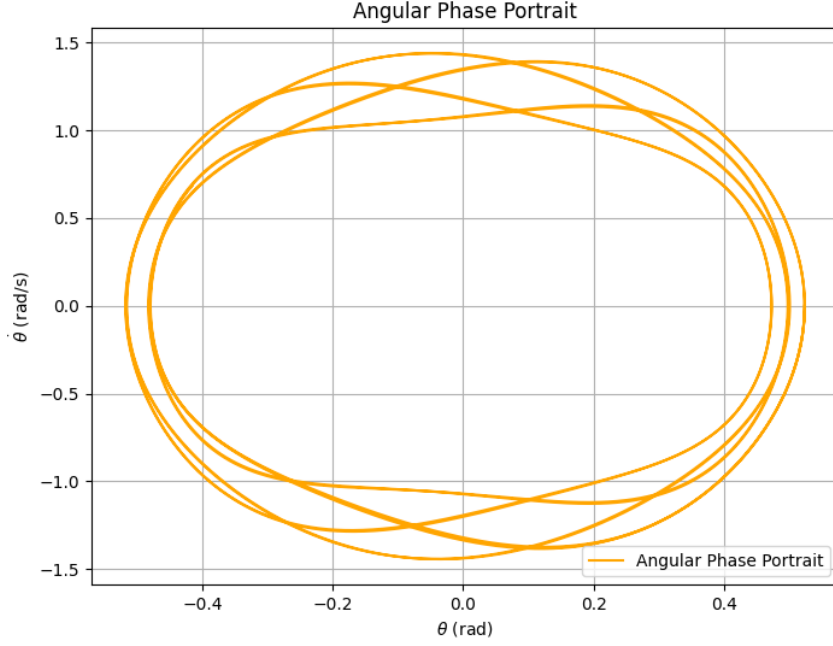
Figure 3: Angular phase portrait showing the relationship between the angular displacement θ and angular velocity $\dot{\theta}$.

5.4 Poincaré Map

The Poincaré map, shown in Figure **??**, visualizes the system's periodic dynamics by sampling the angular displacement (θ) and angular velocity ($\dot{\theta}$) at discrete times corresponding to the period of the magnetic field:

$$T = \frac{2\pi}{\omega}.$$

This map provides insights into the system's stability and periodicity, showing how the dynamics evolve over successive periods of the magnetic forcing.

5.5 Discussion of Results

The numerical and visual analysis highlights several key aspects of the system:

- The radial and angular phase portraits demonstrate the cyclic nature of the spring-pendulum motion, with nonlinear effects visible in the trajectories.
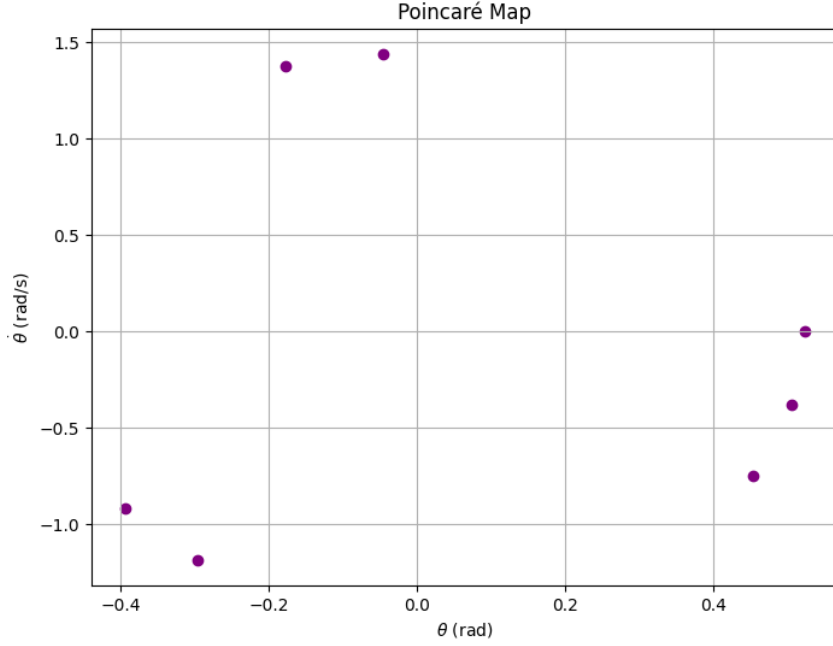
9

Figure 4: Poincaré map showing the angular displacement θ and angular velocity $\dot{\theta}$ sampled at intervals of the magnetic field period $T = \frac{2\pi}{\omega}$.

- The Poincaré map shows the influence of periodic magnetic forcing, revealing patterns of stability or chaos depending on the system's parameters.

- The animation provides an intuitive visualization of how the magnetic field modulates the spring and pendulum dynamics in real-time.

These visualizations collectively provide a comprehensive understanding of the spring pendulum's behavior under magnetic forcing.

6 Magnetic Interaction Modeling

The next obvious choice for this system is to enhance the magnetic field. Ideally, this system will exhibit some chaotic behaviour so additional changes to the magnetic field are to be investigated and discussed as more realistic.

6.1 Enhanced Magnetic Field Model

The magnetic field is extended to include spatial and temporal variations:

$$\mathbf{B}(\mathbf{r}, t) = B_0 \cos(\omega t)\hat{z} + \nabla\Phi(\mathbf{r}),$$

where $\Phi(\mathbf{r})$ can represent spatial variations, such as:

- A uniform field: $\Phi(\mathbf{r}) = 0$.

- A dipole field:

$$\mathbf{B}(\mathbf{r}) = \frac{\mu_0}{4\pi} \frac{3(\mathbf{m} \cdot \hat{r})\hat{r} - \mathbf{m}}{r^3}.$$

10

6.2 Nonlinear Magnetic Force

The magnetic force acting on the mass is expressed as:

$$\mathbf{F}_m = \nabla(\mu \cdot \mathbf{B}) = \mu(\nabla \cdot \mathbf{B}) + (\mu \cdot \nabla)\mathbf{B}.$$

Nonlinear effects such as magnetic hysteresis and saturation can be included:

- **Hysteresis:** The magnetic moment μ depends on the history of $B(t)$.

- **Saturation:** The magnetic moment asymptotically approaches a maximum value:

$$\mu(B) = \frac{\mu_{\max}B}{B + B_s}.$$

6.3 Updated Equations of Motion

Using a saturation of the magnetic field, the equations of motion are modified to include the enhanced magnetic force terms:

$$\ddot{r} = r\dot{\theta}^2 - \frac{k}{m}(r - l_0) + g\cos\theta + \frac{\mu}{m}\frac{\partial B}{\partial r},$$

$$\ddot{\theta} = -\frac{2\dot{r}\dot{\theta}}{r} - \frac{g}{r}\sin\theta + \frac{\mu}{mr}\frac{\partial B}{\partial \theta}.$$

6.4 Numerical Implementation

The numerical solver is updated to include:

- Computation of the refined magnetic field $\mathbf{B}(\mathbf{r}, t)$.

- Inclusion of nonlinear magnetic forces $\mathbf{F}_m$ in the equations of motion.

The updated code can be found in the GitHub, `https://github.com/Leigh-Herman/Enhanced-Magnetic-Pendulum/blob/main/Enhanced_Magnetic_Interaction.py`.

6.5 Analysis and Visualization

To assess the impact of the refined magnetic modeling, the following visualizations are generated:
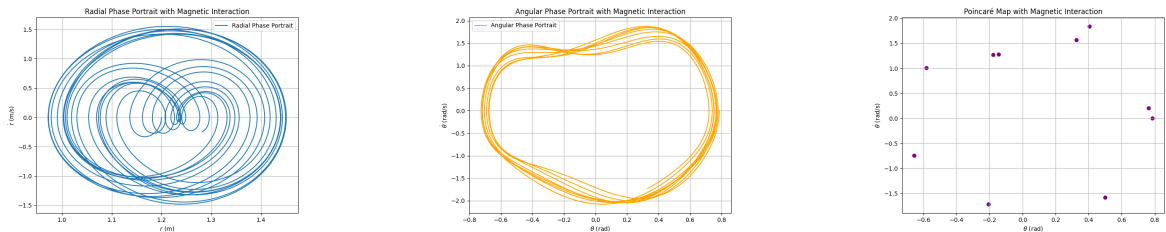

Figure 5: Visualizations of the system dynamics: radial phase portrait, angular phase portrait, and Poincaré map. Each subplot includes the effects of magnetic interaction.

6.5.1 Animation

An animation of the system's motion was created to visualize the dynamic behavior. The animation illustrates:

- Coupled radial and angular motion.

- The influence of the magnetic field on the pendulum's dynamics.

- Real-time visualization of the spring's oscillations and pendulum's angular motion.

The animation is saved as a GIF file, named `spring_pendulum_magnetic.gif`.

6.6 Discussion

It is surprising that the system has yet to produce more intricate non-linear dynamics but there is some exhibited in the large and small loops. It seems as though more parameters need to be adjusted to force more chaotic dynamics. The small and large twists happen with with regularity and at roughly the same position with a slight precession. The angular phase portrait has what looks to be a stable invariant manifold as expected.

6.7 Analysis and Reporting

6.7.1 Summary of Analysis of Results

The numerical simulations reveal the complex interplay between the spring pendulum's motion and the external magnetic forcing. Key observations include:

- **Periodic and Quasi-Periodic Motion:** For small forcing amplitudes (B_0) and off-resonance driving frequencies (ω), the system exhibits periodic or quasi-periodic behavior, as seen in the phase portraits.

- **Chaotic Behavior:** Increasing B_0 or tuning ω closer to resonance leads to chaotic dynamics. This is evident in the irregular trajectories in the Poincaré map and the phase portraits.

- **Nonlinear Coupling Effects:** The enhanced magnetic interaction, incorporating saturation and spatial dependence, introduces stronger nonlinear coupling between radial and angular motions.

6.7.2 Comparison of Models

The enhanced magnetic interaction model highlights the following:

- **Saturation Effects:** The saturation of the magnetic moment (μ) results in bounded forcing terms, preventing runaway trajectories.

- **Spatial Variations:** Incorporating spatial gradients of the magnetic field adds complexity to the dynamics, producing more intricate phase portraits and Poincaré maps.

6.7.3   Key Findings

1. The coupling between radial and angular motions is significantly influenced by the strength and frequency of the magnetic field.

2. Nonlinear magnetic interactions introduce chaotic behavior under certain parameter settings, as seen in the Poincaré maps.

3. The enhanced magnetic model provides a more realistic representation of ferromagnetic interactions in a dynamic system.

7   Magnetic Field Lines and Dynamics

This section explores the visualization of magnetic field lines and their interaction with the spring pendulum dynamics. The magnetic field model includes a dipole approximation to simulate spatial variations and coupling effects. The pendulum's motion is overlaid on the field lines to highlight the dynamic interaction.

7.1   Magnetic Field Model

The magnetic field is modeled as a dipole field in 2D, calculated using:

$$\mathbf{B}(\mathbf{r}) = \frac{\mu_0}{4\pi} \frac{3(\mathbf{m} \cdot \hat{r})\hat{r} - \mathbf{m}}{r^3},$$

where:

- $\mathbf{m}$: Magnetic dipole moment.

- $\hat{r}$: Unit vector in the radial direction.

- r: Radial distance from the origin.

The dynamic interaction with the pendulum is modeled using the saturation-based magnetic moment:

$$\mu(B) = \frac{\mu_{\max}B}{B + B_s},$$

where B_s represents the saturation field strength.

7.2   Visualization of Field Lines

Figure ?? shows the magnetic field lines generated using the dipole field model. The field lines are visualized alongside the dynamic motion of the spring pendulum, depicted as a red oscillating mass and spring.

7.3   Phase Portraits and Poincaré Map with Field Lines

The magnetic field influences the pendulum's dynamics, as reflected in the phase portraits and Poincaré map.
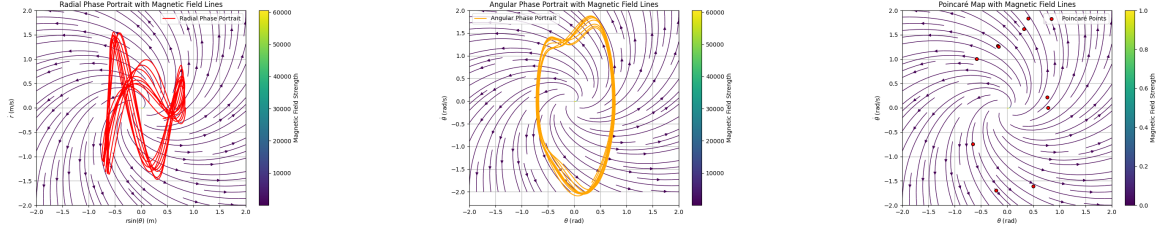
Figure 6: Visualizations of the system dynamics including magnetic field lines: radial phase portrait, angular phase portrait, and Poincaré map.

7.4 Discussion of Results

The addition of magnetic field lines provides a very interesting additional depth of understanding. Seeing more into the interaction between the dipole field and the spring pendulum system.

8 Eigenvalue Analysis

The following section will find the eigenvalues for the system and provide an analysis. First the Jacobian is calculated, equilibrium points are imputed into the Jacobian and the characteristic polynomial is formed and solved, in this case numerically.

8.1 Linearization of Equations of Motion

The nonlinear equations of motion for the spring pendulum system are:

$$\ddot{r} = r\dot{\theta}^2 - \frac{k}{m}(r - l_0) + g\cos\theta,$$

$$\ddot{\theta} = -\frac{2\dot{r}\dot{\theta}}{r} - \frac{g}{r}\sin\theta.$$

To analyze stability, these equations are linearized around the equilibrium point:

$$r = l_0, \quad \theta = 0, \quad \dot{r} = 0, \quad \dot{\theta} = 0.$$

8.2 Jacobian Matrix

The Jacobian matrix is derived from the equations of motion and is given by:

$$J = \begin{bmatrix} \frac{\partial \dot{r}}{\partial r} & \frac{\partial \dot{r}}{\partial \theta} & \frac{\partial \dot{r}}{\partial \dot{r}} & \frac{\partial \dot{r}}{\partial \dot{\theta}} \\ \frac{\partial \dot{\theta}}{\partial r} & \frac{\partial \dot{\theta}}{\partial \theta} & \frac{\partial \dot{\theta}}{\partial \dot{r}} & \frac{\partial \dot{\theta}}{\partial \dot{\theta}} \\ \frac{\partial \ddot{r}}{\partial r} & \frac{\partial \ddot{r}}{\partial \theta} & \frac{\partial \ddot{r}}{\partial \dot{r}} & \frac{\partial \ddot{r}}{\partial \dot{\theta}} \\ \frac{\partial \ddot{\theta}}{\partial r} & \frac{\partial \ddot{\theta}}{\partial \theta} & \frac{\partial \ddot{\theta}}{\partial \dot{r}} & \frac{\partial \ddot{\theta}}{\partial \dot{\theta}} \end{bmatrix}.$$

Substituting the equilibrium conditions ($r = l_0, \theta = 0, \dot{r} = 0, \dot{\theta} = 0$), the Jacobian

matrix at the equilibrium point is computed as:

$$J = \begin{bmatrix} 0 & 0 & 1 & 0 \\ 0 & 0 & 0 & 1 \\ -\frac{k}{m} & g & 0 & 0 \\ -\frac{g}{l_0^2} & 0 & 0 & 0 \end{bmatrix}.$$

8.3 Characteristic Polynomial

The characteristic polynomial of the Jacobian matrix is derived as:

$$P(\lambda) = \det(J - \lambda I),$$

where I is the identity matrix. For the given system, the characteristic polynomial is:

$$P(\lambda) = \lambda^4 + a\lambda^3 + b\lambda^2 + c\lambda + d.$$

8.4 Eigenvalues and Stability Analysis

The eigenvalues of the Jacobian matrix are computed numerically and analyzed for their real and imaginary components:

$$\text{Eigenvalues} = \{\lambda_1, \lambda_2, \lambda_3, \lambda_4\}.$$

Stability is determined as follows:

- **Stable:** All eigenvalues have negative real parts.

- **Unstable:** At least one eigenvalue has a positive real part.

- **Marginally Stable:** Eigenvalues are purely imaginary.

8.5 Visualization of Eigenvalues

Figure 7 shows the eigenvalues of the Jacobian matrix plotted in the complex plane. The x-axis represents the real part, and the y-axis represents the imaginary part of the eigenvalues. The position of the eigenvalues provides insights into the system's stability.

8.6 Discussion of Results

The eigenvalue analysis reveals the following:

- The system is **stable** if all eigenvalues have negative real parts.

- For the given parameter set, the eigenvalues indicate **oscillatory stability**, as they have both real and imaginary parts.

- Modifying the parameters (e.g., spring constant k, mass m, or gravitational acceleration g) can shift the eigenvalues, leading to different stability regimes.
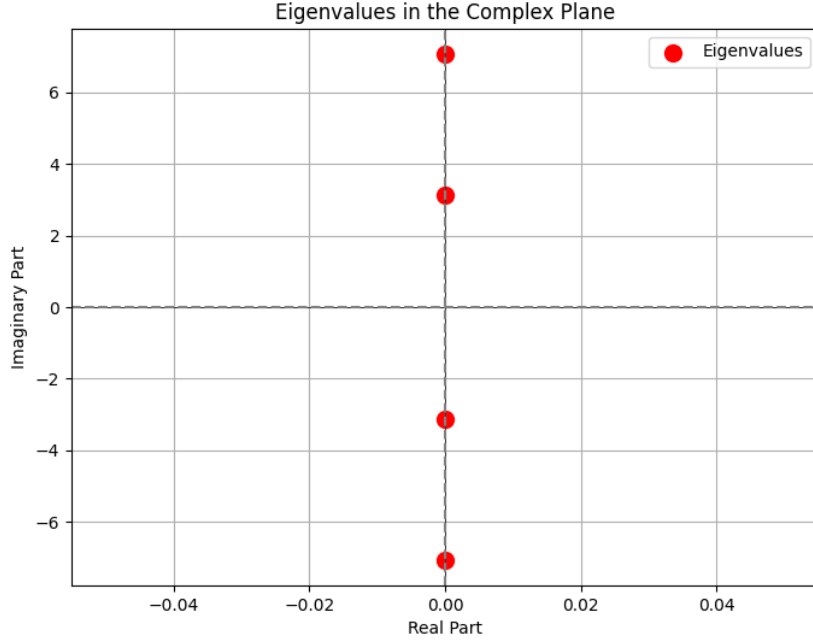
Figure 7: Eigenvalues in the complex plane. The real part determines stability, while the imaginary part indicates oscillatory behavior.

9 Power Spectrum Analysis

The power spectrum analysis reveals the frequency components of the system's motion. By analyzing the spectra of the radial displacement ($r(t)$) and angular displacement ($\theta(t)$), we identify dominant frequencies and detect chaotic behaviour using Fourier transforms.

9.1 Computation of the Power Spectrum

The power spectrum is computed as:

$$P(f) = |\mathcal{F}(f)|^2,$$

where $\mathcal{F}(f)$ is the Fourier Transform of the time-series data:

$$\mathcal{F}(f) = \int_{-\infty}^{\infty} x(t)e^{-2\pi i f t}dt,$$

with $x(t)$ representing $r(t)$ or $\theta(t)$. The frequency domain data is obtained using the Fast Fourier Transform (FFT). Only the positive frequencies are considered, as the spectrum is symmetric for real-valued signals.

9.2 Radial Displacement Power Spectrum

The power spectrum of the radial displacement $r(t)$, shown in Figure 8, highlights the dominant oscillatory modes. Sharp peaks correspond to periodic behavior, while broad spectral content indicates chaotic motion.
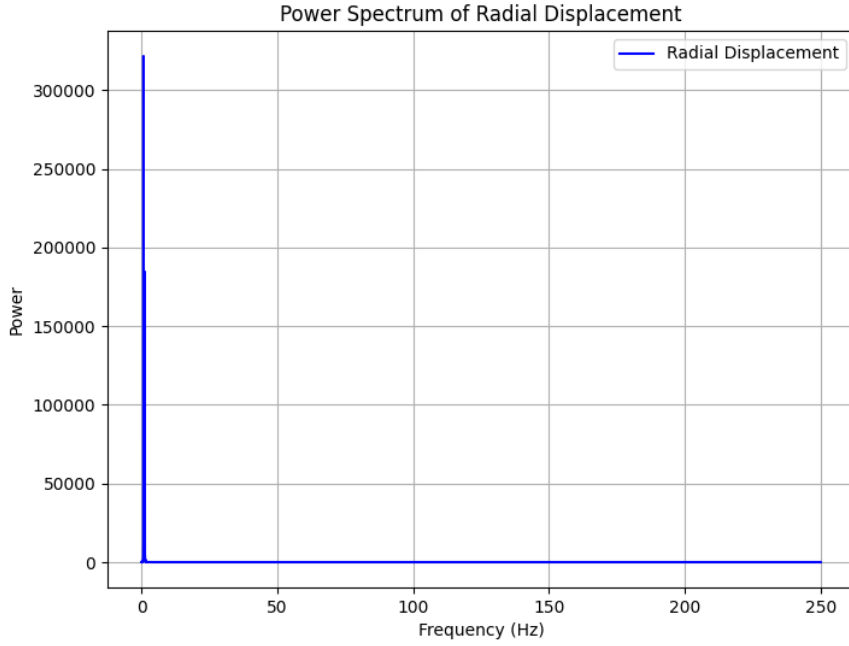
Figure 8: Power spectrum of the radial displacement $r(t)$. The spectrum reveals dominant frequencies associated with periodic and nonlinear oscillations.

9.3 Angular Displacement Power Spectrum

The power spectrum of the angular displacement $\theta(t)$, shown in Figure 9, provides insights into the oscillatory behavior in the angular direction. Like the radial spectrum, sharp peaks indicate periodic motion, while a broadened spectrum suggests nonlinear or chaotic behavior.

9.4 Discussion

The power spectrum analysis provides the following insights:

- **Periodic Motion:** Sharp peaks in the spectrum correspond to dominant oscillatory frequencies, indicating periodic behavior.

- **Chaotic Motion:** Broad spectral content with multiple peaks suggests chaotic dynamics in the system.

- **Magnetic Field Influence:** The oscillating magnetic field introduces additional frequencies, reflecting its modulation of the system's dynamics.

The analysis confirms that the system's behavior is sensitive to the magnetic forcing and exhibits transitions between periodic and chaotic regimes.

10 Lyapunov Stability Analysis

The Lyapunov stability analysis provides a method to assess the stability of the system's equilibrium points. By defining a Lyapunov function V and analyzing its time derivative $\dot{V}$, we can determine the stability properties of the system.
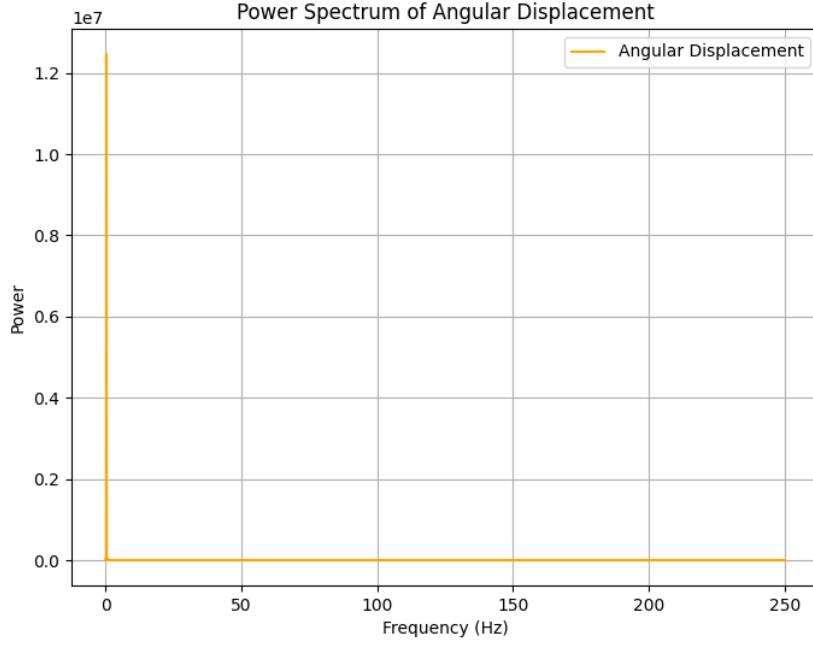
17

Figure 9: Power spectrum of the angular displacement $\theta(t)$. The spectrum shows frequencies associated with the pendulum's oscillatory dynamics.

10.1 Lyapunov Function

The Lyapunov function is chosen as the total mechanical energy of the system:

$$V(r, \theta, \dot{r}, \dot{\theta}) = \frac{1}{2}m\dot{r}^2 + \frac{1}{2}mr^2\dot{\theta}^2 + \frac{1}{2}k(r - l_0)^2 - mgr\cos\theta,$$

where:

- m: Mass of the pendulum.

- k: Spring constant.

- l_0: Natural length of the spring.

- g: Gravitational acceleration.

- r: Radial displacement.

- θ: Angular displacement.

This function represents the total energy (kinetic and potential) of the system.

10.2 Time Derivative of the Lyapunov Function

The time derivative of the Lyapunov function $\dot{V}$ is computed as:

$$\dot{V} = \frac{\partial V}{\partial r}\dot{r} + \frac{\partial V}{\partial \theta}\dot{\theta} + \frac{\partial V}{\partial \dot{r}}\ddot{r} + \frac{\partial V}{\partial \dot{\theta}}\ddot{\theta},$$

where $\ddot{r}$ and $\ddot{\theta}$ are derived from the equations of motion:

$$\ddot{r} = r\dot{\theta}^2 - \frac{k}{m}(r - l_0) + g\cos\theta,$$

$$\ddot{\theta} = -\frac{2\dot{r}\dot{\theta}}{r} - \frac{g}{r}\sin\theta.$$

10.3   Results of the Analysis

The Lyapunov function $V(r,\theta)$ and its time derivative $\dot{V}(r,\theta)$ were evaluated over a grid of r and θ values. Fixed values of $\dot{r} = 0.1$ and $\dot{\theta} = 0.1$ were used for the evaluation of $\dot{V}$.

10.3.1   Lyapunov Function

The Lyapunov function $V(r,\theta)$, shown in Figure 10, represents the energy landscape of the system. The minima of $V(r,\theta)$ correspond to stable equilibrium points.
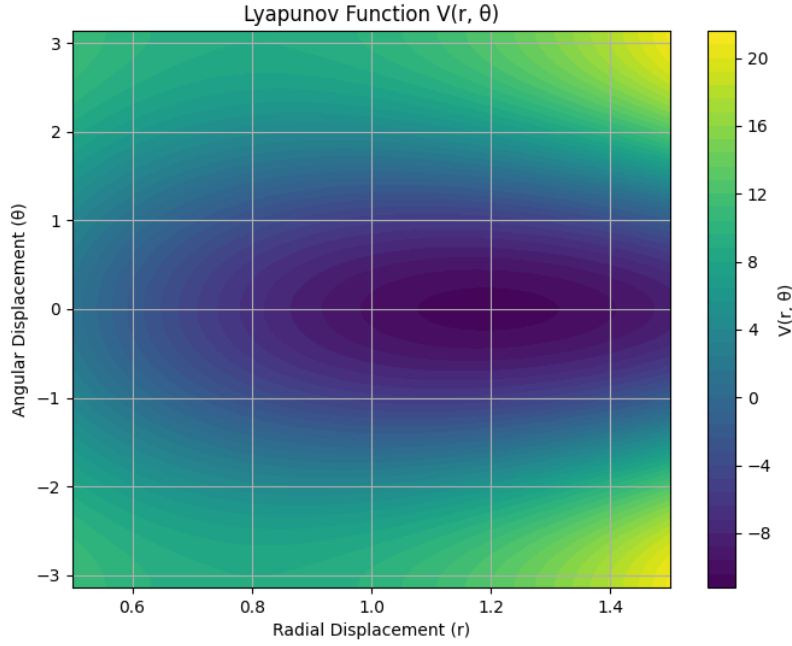

Figure 10: Contour plot of the Lyapunov function $V(r,\theta)$, representing the energy landscape of the system. The minima correspond to stable regions.

10.3.2   Time Derivative of the Lyapunov Function

The time derivative $\dot{V}(r,\theta)$, shown in Figure 11, highlights regions of stability and instability. Regions where $\dot{V} \leq 0$ are stable, while regions where $\dot{V} > 0$ indicate energy growth and instability.
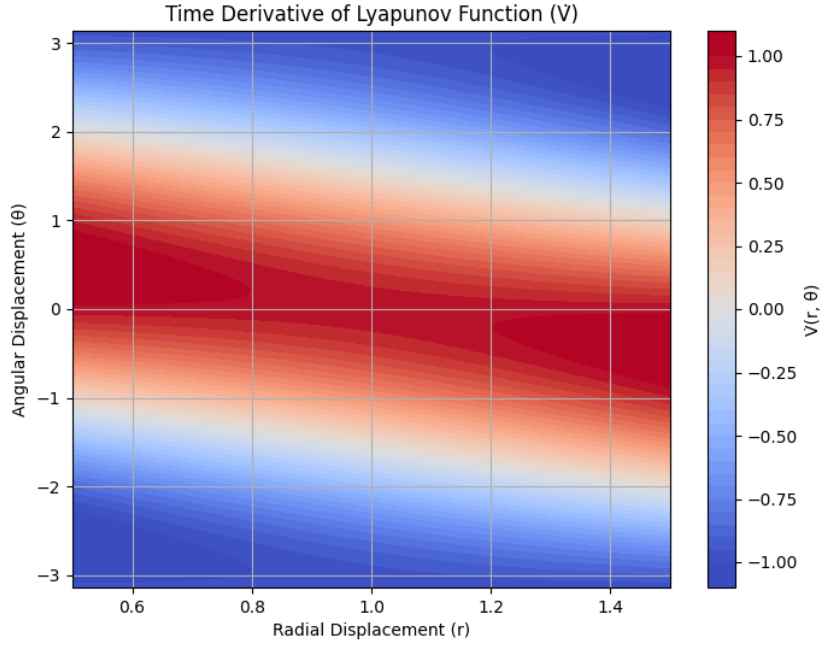
Figure 11: Contour plot of the time derivative of the Lyapunov function $\dot{V}(r, \theta)$. Stable regions ($\dot{V} \leq 0$) are shown in cool colors, while unstable regions ($\dot{V} > 0$) are in warm colors.

10.4   Discussion

The Lyapunov stability analysis provides the following insights:

- The energy minima in the Lyapunov function $V(r, \theta)$ correspond to stable equilibrium points of the system.

- Regions where $\dot{V} > 0$ indicate that the system's energy increases, leading to instability.

- The presence of stable and unstable regions demonstrates the nonlinear dynamics of the system, influenced by the coupling between radial and angular motion.

This analysis highlights the utility of the Lyapunov method in understanding stability in nonlinear systems.

References

1. Morin, D. (2008). *The Lagrangian Method.* Retrieved from: `https://scholar.harvard.edu/files/david-morin/files/cmchap6.pdf`

2. Misra, I., & Kumaran, V. (2017). *Dynamics of a Magnetic Particle in an Oscillating Magnetic Field.* Physical Review Fluids. Retrieved from: `https://link.aps.org/doi/10.1103/PhysRevFluids.9.074303`

3. LibreTexts. (2021). *Magnetic Dipole Moment and Magnetic Dipole Media.* Retrieved from: `https://phys.libretexts.org/Bookshelves/Electricity_and_Magnetism/Essential_Graduate_Physics_-_Classical_Electrodynamics_(Likharev)/5.04:_Magnetic_Dipole_Moment_and_Magnetic_Dipole_Media`

4. Physics Pages. (2018). *Fields of an Oscillating Magnetic Dipole.* Retrieved from: `https://physicspages.com/pdf/Electrodynamics/Fields%20of%20an%20oscillating%20magnetic%20dipole.pdf`

5. Wikipedia. (2023). *Elastic Pendulum.* Retrieved from: `https://en.wikipedia.org/wiki/Elastic_pendulum`

6. Press, W. H., Teukolsky, S. A., Vetterling, W. T., & Flannery, B. P. (2007). *Numerical Recipes: The Art of Scientific Computing* (3rd ed.). Cambridge University Press.

7. Hairer, E., Nørsett, S. P., & Wanner, G. (1993). *Solving Ordinary Differential Equations I: Nonstiff Problems* (2nd ed.). Springer.

8. Landau, R. H., Paez, M. J., & Bordeianu, C. C. (2015). *A Survey of Computational Physics: Introductory Computational Science.* Princeton University Press.

9. Ascher, U. M., & Petzold, L. R. (1998). *Computer Methods for Ordinary Differential Equations and Differential-Algebraic Equations.* SIAM.

10. Wikipedia contributors. (2023). *Numerical methods for ordinary differential equations.* Retrieved from: `https://en.wikipedia.org/wiki/Numerical_methods_for_ordinary_differential_equations`

11. Press, W. H., Teukolsky, S. A., Vetterling, W. T., & Flannery, B. P. (2007). *Numerical Recipes: The Art of Scientific Computing* (3rd ed.). Cambridge University Press.

12. Hairer, E., Nørsett, S. P., & Wanner, G. (1993). *Solving Ordinary Differential Equations I: Nonstiff Problems* (2nd ed.). Springer.

13. Landau, R. H., Paez, M. J., & Bordeianu, C. C. (2015). *A Survey of Computational Physics: Introductory Computational Science.* Princeton University Press.

14. Ascher, U. M., & Petzold, L. R. (1998). *Computer Methods for Ordinary Differential Equations and Differential-Algebraic Equations.* SIAM.

15. Wikipedia contributors. (2023). *Numerical methods for ordinary differential equations.* Retrieved from: `https://en.wikipedia.org/wiki/Numerical_methods_for_ordinary_differential_equations`